μ-Pyrazolato-μ-carboxylato- and Di(μ-pyrazolato)-dimanganese(II) Complexes: Synthesis, Characterization and Catalase-like Function†

Makoto Itoh, Ken-ichiro Motoda, Kenji Shindo, Toshiro Kamiusuki, Hiroshi Sakiyama, Naohide Matsumoto and Hisashi Ōkawa*

Department of Chemistry, Faculty of Science, Kyushu University, Hakozaki, Higashiku, Fukuoka 812, Japan

3,5-Bis[*N*,*N*-di(2-pyridylmethyl)aminomethyl]pyrazole (HL^1) and 3,5-bis[*N*,*N*-bis(2-diethylaminoethyl)aminomethyl]pyrazole (HL^2) formed μ-pyrazolato-μ-carboxylato-dimanganese(II) complexes $[Mn_2L(O_2CR)][BPh_4]_2$ (L = L^1, R = Ph; **1**; L = L^2, R = Me **2**) and 3,5-bis[*N*-(2-pyridylmethyl)-aminomethyl]pyrazole (HL^3) gave a di(μ-pyrazolato)-dimanganese(II) complex $[Mn_2L^3_2][BPh_4]_2$ **3**. The ditoluene adduct of **3** crystallizes in the triclinic space group $P\bar{1}$ with a = 14.452(3), b = 15.573(5), c = 10.988(4) Å, α = 108.78(3), β = 93.31(2) and γ = 115.10(2)°. X-Ray diffraction analysis revealed a di(μ-pyrazolato)-dimanganese(II) core with Mn···Mn separation 4.181(2) Å. All the complexes showed catalytic activity towards disproportionation of H_2O_2 in dimethylformamide at 0 °C. The initial rate of dioxygen evolution in the presence of **1** is first order in both the complex concentration and that of H_2O_2; $v = k[Mn_2][H_2O_2]$, k = 1.45 $dm^3\ mol^{-1}\ s^{-1}$. Together with the observation of a ligand-to-metal charge-transfer band characteristic of Mn^{IV}=O in the catalysis by **2**, a mechanistic scheme involving a cycle from $\{Mn^{III}(OH)\}_2$ to $\{Mn^{IV}(=O)\}_2$ is inferred. In the disproportionation by **3** the initial rate of evolution is first order in complex concentration and second order in that of H_2O_2; $v = k[Mn_2][H_2O_2]^2$, k = 29 $dm^6\ mol^{-2}\ s^{-1}$).

It is known[1] that some metallobiosites contain a pair of metal ions in close proximity. Recent extended X-ray absorption fine structure (EXAFS) and X-ray crystallographic studies have revealed a metal–metal separation of 3.2–4.3 Å for bimetallic biosites and in some such as haemocyanin (Cu···Cu 3.6–3.7 Å)[2] and manganese catalases (Mn···Mn ≈3.6 Å)[3] the intermetallic separation is evidently essential for incorporating substrate (O_2 or H_2O_2) between a pair of metal ions. Therefore, the design of dinuclear core complexes with an appropriate metal–metal separation is very important in studies on functional models for those bimetallic biosites.

Pyrazoles,[4–8] 1,2,4-triazoles,[6,9] pyridazines[5,10–12] and phthalazines[5,10,13] are able to bridge two metal ions through the diazine (=N–N=) group. Dinuclear metal complexes bridged by diazines are particularly of interest because these bridges provide a metal–metal separation of 3.5–4.5 Å relevant to bimetallic biosites. Previously[14–18] we have reported pyrazole-based dinucleating ligands possessing two chelating arms attached to the 3 and 5 positions of the pyrazole ring. The compound 3,5-bis[*N*,*N*-bis(2-diethylaminoethyl)aminomethyl]-pyrazole forms L:M = 1:2 type dinuclear copper(II) complexes where a pair of copper(II) ions are bridged by the endogenous pyrazolate group and an exogenous azide or acetate group.[16] 3,5-Bis[*N*-(2-diethylaminoethyl)aminomethyl]pyrazole forms a 2:2 type dinuclear complex having a di(μ-pyrazolato)-dicopper(II) core [Cu···Cu 3.903(2) Å].[15] Manganese complexes of those pyrazole-based ligands are very interesting as models of dimanganese biosites such as manganese catalases. In this study new pyrazole-based compounds possessing a pyridyl group as the pendant donor, 3,5-bis[*N*,*N*-di(2-pyridylmethyl)aminomethyl]pyrazole and 3,5-bis[*N*-(2-pyridylmethyl)aminomethyl]pyrazole, are prepared and used together with the previous ones with a pendant diethylamino group to obtain manganese complexes.

Two types of dinuclear complexes, $[MnL(O_2CR)][BPh_4]_2$ (L = L^1, R = Ph **1**; L = L^2, R = Me **2**) and $[Mn_2L^3_2][BPh_4]_2$ **3**, have been derived and the crystal

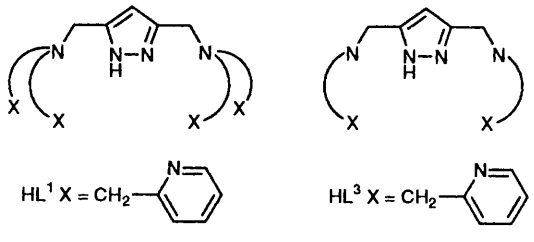

structure of the ditoluene adduct **3**·$2C_6H_5Me$ determined by X-ray crystallography. The main emphasis of this study is placed on the catalase-like activity of **1**–**3** to disproportionate hydrogen peroxide.

Experimental

Measurements.—Elemental analyses of carbon, hydrogen and nitrogen were obtained from the Service Centre of Elemental Analysis of Kyushu University. Analyses of Mn were made on a Shimadzu AA-680 atomic absorption/flame emission spectrophotometer. Fast atom bombardment (FAB) mass spectra were recorded on a JEOL JMS-SX102A mass spectrometer, Infrared spectra on a JASCO IR-810 spectrophotometer using KBr discs or Nujoll mulls and electronic spectra in dimethylformamide (dmf) on a Shimadzu MPS-2000 spectrophotometer. An Oxford DN1704 nitrogen-bath cryostat controlled by an Oxford ITC4 temperature controller was used for measurements of electronic spectra at low temperature.

† *Supplementary data available:* see Instructions for Authors, *J. Chem. Soc., Dalton Trans.*, 1995, Issue 1, pp. xxv–xxx.

Non-SI unit employed: $\mu_B \approx 9.27 \times 10^{-24}$ J T^{-1}.

Solid-state magnetic susceptibilities were determined on a Faraday balance in the temperature range 80–300 K and on a HOXAN HSM-D SQUID susceptometer in the range 4.2–80 K. The apparatus were calibrated with $[Ni(en)_3][S_2O_3]$[19] (en = ethane-1,2-diamine) and diamagnetic corrections for constituent atoms were made using Pascal's constants.[20] Cyclic voltammograms were recorded in dmf using a three-electrode cell equipped with a glassy carbon working electrode, a platinum coil as the counter electrode, and a saturated calomel electrode (SCE) as the reference. Tetra(*n*-butyl)ammonium perchlorate was used as the supporting electrolyte. **CAUTION**: this perchlorate is explosive and should be handled with great care!)

Materials.—Pyrazole-3,5-dicarboxylic acid was obtained from Aldrich Chem. Co. and di(2-pyridylmethyl)amine from Nacharai Chem. Co. 3,5-Di(aminomethyl)pyrazole dihydrochloride[14] and 3,5-di(aminomethyl)pyrazole[17] were prepared by the literature methods. The syntheses of HL^2 and HL^4 were described previously.[15,16]

Preparations.—3,5-*Bis*[N,N-*di*(2-*pyridylmethyl*)*aminomethyl*]*pyrazole* (HL^1). A mixture of 3,5-di(chloromethyl)pyrazole hydrochloride (300 mg, 1.5 mmol) and di(2-pyridylmethyl)-amine (598 mg, 3 mmol) was stirred at room temperature for 2 h. It was then shaken with chloroform (50 cm^3), and the chloroform solution washed with two portions (20 cm^3) of water, dried over Na_2SO_4, and evaporated to dryness to give crude HL^1 as a colourless oily substance. This was used for the preparation of manganese complexes without further purification.

3,5-*Bis*[N-(2-*pyridylmethyl*)*aminomethyl*]*pyrazole* (HL^3). A methanol solution of 3,5-di(aminomethyl)pyrazole dihydrochloride (300 mg, 1.5 mmol) was neutralized with lithium hydroxide monohydrate (126 mg, 3 mmol). To this was added a solution of 2-pyridine-2-carbaldehyde (321 mg, 3 mmol) in methanol (10 cm^3) and the mixture stirred at room temperature for 10 min. Then an excess of $NaBH_4$ (*ca.* 500 mg) was added little by little with vigorous stirring. The reaction mixture was treated with water (10 cm^3) and shaken with three portions (50 cm^3) of chloroform. The combined chloroform solution was washed with water (*ca.* 100 cm^3), dried over Na_2SO_4, and evaporated to dryness to give crude HL^3 as a pale yellow oily substance. This was used for the preparation of manganese complexes without further purification.

$[Mn_2L^1(O_2CPh)][BPh_4]_2$·dmf **1**. In an atmosphere of argon a solution of HL^1 (730 mg, 1.5 mmol) and triethylamine (2 cm^3) in methanol (10 cm^3) was mixed with a solution of manganese(II) benzoate tetrahydrate (1.1 g, 3 mmol) in the minimum volume of methanol, and the mixture stirred at ambient temperature for 15 min. The addition of a methanolic solution of sodium tetraphenylborate (1.0 g, 3 mmol) resulted in the precipitation of pale microcrystals. These were dissolved in dmf and the solution was diffused with methanol to give colourless needles. Yield: 115 mg (5%) (Found: C, 72.90; H, 5.70; Mn, 7.65; N, 8.50. Calc for $C_{87}H_{81}B_2Mn_2N_9O_3$: C, 72.95; H, 5.70; Mn, 7.65; N, 8.80%). Effective magnetic moment (μ_{eff}/μ_B) per Mn: 5.72. Molar conductance (Λ_M/S cm^2 mol^{-1}) in dmf: 81. Selected IR data $\tilde{\nu}/cm^{-1}$) for KBr disc: 3049, 3026, 2995, 2975, 1655, 1603, 1543, 1478, 1404, 1255, 1155, 1097, 1018, 839, 760, 732, 702 and 608.

$[Mn_2L^2(O_2CMe)][BPh_4]_2$·MeOH **2**. A solution of HL^2 (55 mg, 1×10^{-4} mol) and manganese(II) acetate tetrahydrate (50 mg, 1×10^{-4} mol) in methanol (10 cm^3) was stirred in argon atmosphere at ambient temperature. The pH was adjusted to 7 by adding triethylamine. Addition of a methanolic solution of sodium tetraphenylborate (70 mg, 2×10^{-4} mol) resulted in the precipitation of white microcrystals. They were recrystallized from dichloromethane–methanol (1:1 v/v). Yield: 110 mg (79%) (Found: C, 70.60; H, 8.00; Mn, 8.05; N, 8.05;. Calc. for $C_{80}H_{108}B_2Mn_2N_8O_3$: C, 70.60; H, 8.00; Mn, 8.05; N, 8.25%). Effective magnetic moment (μ_{eff}/μ_B) per Mn: 5.89. Molar conductance (Λ_M/S cm^2 mol^{-1}) in dmf: 80. Selected IR data ($\tilde{\nu}/cm^{-1}$) for KBr disc: 3049, 2975, 2918, 2868, 1565, 1478, 1443, 1428, 1382, 1261, 1181, 1138, 1107, 1037, 738, 708 and 607.

$[Mn_2L^3_2][BPh_4]_2$·MeOH **3**·MeOH. To a solution of HL^3 (460 mg, 1.5 mmol) in methanol (10 cm^3) was added a methanolic solution of Na(OMe) (prepared by dissolving 100 mg metallic sodium in 20 cm^3 methanol), and the mixture was stirred for 1 h at room temperature. To this were successively added a solution of manganese(II) benzoate tetrahydrate (550 mg, 1.5 mmol) in methanol (*ca.* 20 cm^3) and a solution of sodium tetraphenylborate (513 mg, 1.5 mmol) in methanol (*ca.* 10 cm^3), resulting in the precipitation of a pale coloured powder. It was crystallized from acetone–methanol (1:1 v/v) to form colourless microcrystals. The yield was 340 mg (24%) (Found: C, 71.40; H, 5.95; Mn, 7.85; N, 11.80. Calc. for $C_{83}H_{82}B_2Mn_2N_{12}O$: C, 71.45; H, 5.90; Mn, 7.90; N, 12.05%. Effective magnetic moment (μ_{eff}/μ_B) per Mn: 5.85. Molar conductance (Λ_M/S cm^2 mol^{-1}) in dmf: 76. Selected IR data ($\tilde{\nu}/cm^{-1}$) for KBr disc: 3297, 3052, 3000, 2900, 1604, 1580, 1572, 1480, 1442, 1427, 1053, 1033, 1017, 737, 707 and 615.

A portion was dissolved in acetonitrile and the solution was diffused with toluene. After 1 week single crystals of $[Mn_2L^3_2][BPh_4]_2$·$2C_6H_5Me$, suitable for X-ray structural analysis, were grown (Found: C, 74.50; H, 6.10; Mn, 7.1; N, 10.85. Calc. for $C_{96}H_{94}B_2Mn_2N_{12}$: C, 74.50; H, 6.10; Mn, 7.15, N, 10.85%).

X-Ray Structure Analysis of $[Mn_2L^3_2][BPh_4]_2$·$2C_6H_5Me$. —A crystal with approximate dimensions 0.4 × 0.4 × 0.3 mm, mounted on a glass fibre and coated with epoxy resin, was used. Intensities and lattice parameters were obtained at 20 °C on a Rigaku AFC7R automated four-circle diffractometer with graphite-monochromated Mo-Kα radiation (λ = 0.710 69 Å) and a 12 kW rotating-anode generator. Lattice parameters were obtained from a least-squares fit to 25 reflections in the range $28 < 2\theta < 30°$. Crystal data are summarized in Table 1. The intensity data were collected by the ω–2θ scan technique to a maximum 2θ value of 50°. The octant measured was $+h$, $\pm k$, $\pm l$ (0–17, −19 to 19, −13 to 13). Scans of $(1.68 + 0.30 \tan\theta)°$ were made at a speed of 16.0° min^{-1} in ω. The weak reflections [$I < 10.0\sigma(I)$] were rescanned and the counts accumulated to ensure good counting statistics.

Of the 7571 reflections collected, 7258 reflections were found to be unique (R_{int} = 0.047). Three standard reflections were monitored every 150 and showed 0.6% decrease in intensity over the course of data collection. A linear correction factor was applied to the data to account for this. An empirical absorption correction based on azimuthal scans of several reflections was applied, resulting in transmission factors ranging from 0.93 to 1.00. The data were corrected for Lorentz and polarization effects.

The structure was solved by the direct method and expanded using Fourier techniques. The function minimized was $\Sigma w(|F_o| - |F_c|)^2$ with $w = 1/\sigma^2(F_o)$. The non-hydrogen atoms were refined anisotropically. Hydrogen atoms were fixed at calculated positions and included in the structure-factor calculation but not refined. The final cycle of full-matrix least-squares refinement was based on 5492 observed reflections [$I > 3.00\sigma(I)$] and 506 variable parameters and converged with unweighted (R) and weighted (R') agreement factors of 0.058 and 0.066, respectively.

Neutral atom scattering factors were taken from ref. 21. Anomalous dispersion effects were included in the final calculation;[22] the values for $\Delta f'$ and $\Delta f''$ were taken from ref. 23. The values for the mass-attenuation coefficients were taken from ref. 24. All the calculations were carried out on an IRIS indigo computer by use of the TEXSAN crystallographic software package.[25] The final positional parameters of non-hydrogen atoms with their estimated standard deviations are listed in Table 2.

Additional material available from the Cambridge Crystallographic Data Centre comprises H-atom coordinates, thermal parameters and remaining bond lengths and angles.

Catalase-like Activity.—A closed vessel containing a dmf solution (2 cm^3) of a dinuclear manganese(II) complex (5×10^{-6} mol) was stirred at 0 °C on an ice–water bath. Hydrogen peroxide (9.9%, 0.5 cm^3, 1.45 mmol) chilled at 0 °C was injected by the use of a microsyringe through a silicon stopper and the dioxygen evolved was measured volumetrically with a burette. Kinetic studies were made using the same device by changing the complex or H_2O_2 concentration.

Results and Discussion

Preparation and General Characterization.—In the preparation of HL^2 and HL^4 [15,16] the amide precursors 3,5-bis[*N*,*N*-bis(2-diethylaminoethyl)carbamoyl]pyrazole and 3,5-bis[*N*-(2-diethylaminoethyl)carbamoyl]pyrazole, respectively, were reduced with $LiAlH_4$. This method could not be applied to the preparation of HL^1 and HL^3 because the reduction of their amide precursors 3,5-bis[*N*,*N*-di(2-pyridylmethyl)carbamoyl]-pyrazole and 3,5-bis[*N*-(2-pyridylmethyl)carbamoyl]pyrazole, respectively, with $LiAlH_4$ resulted in cleavage of the CO–N bond. In this study HL^1 was prepared by the reduction by $NaBH_4$ of 3,5-di[*N*-(2-pyridylmethyl)iminomethyl]pyrazole prepared by condensation of 3,5-di(aminomethyl)pyrazole and 2-formylpyridine. The compound HL^3 was obtained by reaction of 3,5-di(chloromethyl)pyrazole and di(2-pyridylmethyl)amine.

Compounds HL^1 and HL^2, possessing two pendant groups on each articular nitrogen, provided the dinuclear manganese(II) complexes of L:Mn = 1:2 type, $[Mn_2L^1(O_2CPh)][BPh_4]_2$·dmf **1** and $[Mn_2L^2(O_2CMe)][BPh_4]_2$·MeOH **2**, respectively. It is presumed that in each complex the pyrazolate group acts as the endogenous bridge and the carboxylate group as the exogenous bridge. Evidence in support of the carboxylate bridge is provided by the small separation (< 200 cm^{-1}) between the antisymmetric and symmetric stretching modes of the carboxylate group,[26] $\nu_{asym}(CO_2)$ 1543 and $\nu_{sym}(CO_2)$ 1404 cm^{-1} for **1** and ν_{asym}1565 and ν_{sym}1443 cm^{-1} for **2**. Compound HL^3 possessing one pendant group on each articular nitrogen formed a dinuclear manganese(II) complex of the L:Mn = 2:2 type, $[Mn_2L^3{}_2][BPh_4]_2$·MeOH **3**. It has a di(μ-pyrazolato)-dimanganese(II) core structure as discussed below. Compound HL^4 formed a similar di(μ-pyrazolato)-dimanganese(II) core complex which, however, was not included in this study because of contamination from an impurity.

All the complexes act as electrolytes in dmf (Λ_M 76–81 S cm^2 mol^{-1}). The molar conductances are significantly smaller than those reported for 2:1 electrolytes (130–170 S cm^2 mol^{-1})[27] probably due to the large cations.

All the complexes are colourless and show no absorption in the near-ultraviolet and visible regions, in accord with the high-spin manganese(II) ion involved. The high-spin electronic configuration in **1–3** has been confirmed by magnetic measurements. The temperature dependences of the magnetic susceptibility and effective magnetic moment of **1** (per Mn) are shown in Fig. 1. The effective magnetic moment of **1** is 5.72 μ_B (per Mn) at room temperature and decreases with decreasing temperature, suggesting an antiferromagnetic interaction between a pair of manganese(II) ions. Magnetic analyses have been made using the magnetic susceptibility expression (1)

$$\chi_A = (Ng^2\beta^2/kT)(A/B) \quad (1)$$

based on the isotropic Heisenberg model ($H = -2JS_1 \cdot S_2$) for ($S_1 = S_2 = \frac{5}{2}$), where $A = x^{28} + 5x^{24} + 14x^{18} + 30x^{10} + 55$, $B = x^{30} + 3x^{28} + 5x^{24} + 7x^{18} + 9x^{10} + 11$, and $x = \exp(-J/kT)$; the other symbols have their usual meanings. The cryomagnetic property of **1** is well reproduced by this expression as indicated by the trace in Fig. 1, using $g = 1.95$ and $J = -0.25$ cm^{-1}. The discrepancy factor defined as $R(\chi) = [\Sigma(\chi_{obs} - \chi_{calc})^2/\Sigma(\chi_{obs})^2]$ was 1.3×10^{-3}. Similarly, the cryomagnetic properties of **2** and **3** have been simulated by expression (1) using $g = 2.00$ and $J = -0.37$ cm^{-1} for **2** [$R(\chi) = 5.9 \times 10^{-4}$] and $g = 2.00$ and $J = -0.40$ cm^{-1} for **3** [$R(\chi) = 7.6 \times 10^{-4}$]. The estimated error in these best-fittings is ±0.01 for g and ±0.02 cm^{-1} for J.

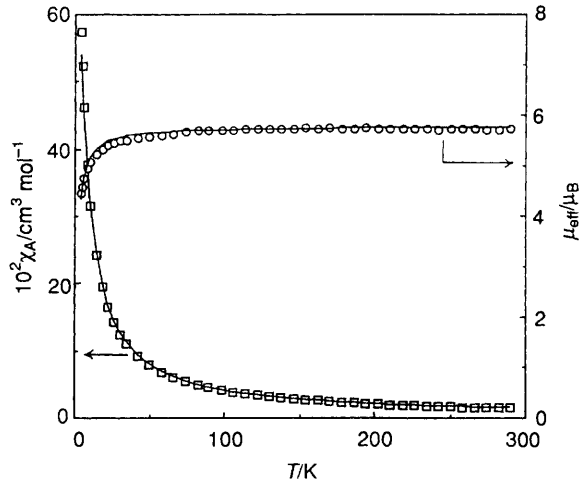

Fig. 1 Temperature dependences of the magnetic susceptibility (□) and effective magnetic moment (○) of complex **1**

The electrochemical properties of complexes **1–3** have been studied by cyclic voltammetry in dmf at a glassy-carbon working electrode. Complex **1** showed an irreversible wave exhibiting only an anodic peak at +1.06 V (*vs.* SCE). Complex **2** also showed an irreversible wave with only the anodic peak at +0.80 V. Complex **3** showed two anodic peaks at +0.38 and +1.06 V *vs.* SCE; the corresponding cathodic peaks were not observed in the sweep up to +1.2 V. In the sweep in the range of 0 to +0.6 V, on the other hand, the first wave was quasi-reversible (E_{ap} = +0.38 and E_{cp} = +0.28 V) and involved one-electron transfer according to coulometry at +0.3 V.

None of the complexes showed a reduction wave at the available potentials.

Crystal Structure of $[Mn_2L^3{}_2][BPh_4]_2$·$2C_6H_5Me$.—An ORTEP[28] view of the complex cation with atom numbering scheme is shown in Fig. 2. Selected bond distances and angles are given in Table 3. The complex cation consists of two ligands $(L^3)^-$ and two manganese ions: two tetraphenylborate ions and two toluene molecules are captured in the crystal lattice. The two metal ions are bridged by two pyrazolate ions with a Mn ··· Mn separation of 4.181(2) Å. There is an inversion centre at the centre of the di(μ-pyrazolato)-dimanganese(II) core. The geometrical environment about each Mn is regarded as a distorted octahedron with two pyrazolate nitrogens [N(3) and N(4*)] and two articular nitrogens [N(2) and N(5*)] on the basal plane and two pyridyl nitrogens [N(1) and N(6*)] at the axial sites.

All the Mn–N bond distances are longer than 2.1 Å in accord with the high-spin manganese(II) oxidation state. The Mn(1)–N(2) and Mn(1)–N(5*) are significantly elongated [2.406(4) and 2.426(4) Å, respectively] probably due to a strain in the dinuclear core. A similar deformation is seen in the di(μ-pyrazolato)-dicopper(II) core of a $(L^4)^-$ complex.[17] The most noticeable feature in the present complex is the co-ordination attitude of the pendant pyridyl groups. That is, two pyridyl nitrogens N(1) and N(6) of one ligand, co-ordinated to Mn(1) and Mn(1*), respectively, are situated on the same side with respect to the plane of the di(μ-pyrazolato)-dimanganese(II) core. This differs from the co-ordination attitude of the pendant

group in the di(μ-pyrazolato)-dicopper(II) core of the $(L^4)^-$ complex.[17] In that case each Cu^{II} assumes a square-pyramidal geometry with a pendant nitrogen at the axial site but the two pendant nitrogens in one ligand are situated at different sides of the core plane.

Catalase-like Function.—The catalase-like function of complexes **1–3**, decomposing hydrogen peroxide, has been studied in dmf at 0 °C. The time courses of the dioxygen evolution are shown in Fig. 3. The total amount of dioxygen evolved corresponds to 0.5 molar equivalent of the added hydrogen peroxide in all cases, indicating the catalytic disproportionation of H_2O_2. The disproportionation reaction with **1** is significantly slower than that with **2**. Complex **3** shows a high catalytic activity compared with those of **1** and **2**.

In the catalytic disproportionation by complex **1** the initial rate of dioxygen evolution is dependent upon both the complex concentration and that of H_2O_2: evolution profiles at different complex concentrations are shown in Fig. 4. When the initial rate is plotted against the complex concentration a good linear correlation is established as shown in Fig. 5(*a*). Similarly, the initial rate of evolution is linearly correlated to the concentration of H_2O_2 as shown in Fig. 6. Thus, the apparent initial rate of disproportionation of H_2O_2 is first order to both the complex concentration and that of H_2O_2; *i.e.* $v = k$[complex][H_2O_2] with $k = 1.45$ dm^3 mol^{-1} s^{-1}. This suggests the involvement of a 1:1 adduct of **1** and H_2O_2. The rate constant is very small compared to that of the native catalases.[29,30]

In the disproportionation of H_2O_2 by complex **1** the reaction mixture became brown. On cooling to −50 °C the evolution of O_2 practically ceased, allowing us to measure the absorption spectrum [Fig. 7(*a*)]. Despite the very poor resolution, the spectrum suggests the involvement of a higher oxidation state of manganese-(III) or -(IV) in the catalytic process; **1** itself shows no absorption as shown in Fig. 7(*b*). In the corresponding disproportionation with **2** the reaction mixture at −50 °C was brownish purple and exhibited a significantly intense absorption at ≈520 nm upon which fine structure, separated by

Table 1 Crystal data for $[Mn_2L^3{}_2][BPh_4]_2 \cdot 2C_6H_5Me$

Formula	$C_{96}H_{94}B_2Mn_2N_{12}$
Colour	Pale yellow
M	1547.37
Crystal system	Triclinic
Space group	$P\bar{1}$
a/Å	14.452(3)
b/Å	15.573(5)
c/Å	10.988(4)
α/°	108.78(3)
β/°	93.31(2)
γ/°	115.10(2)
U/Å^3	2064(1)
Z	1
D_m/g cm^{-3}	1.25
D_c/g cm^{-3}	1.244
μ(Mo-Kα)/cm^{-1}	3.61
No. of reflections measured	7258
No. of reflections observed[a]	5492
R[b]	0.058
R'[c]	0.066

[a] With $|F_o| > 3\sigma(|F_o|)$. [b] $\Sigma||F_o| - |F_c||/\Sigma|F_o|$. [c] $[\Sigma w(|F_o| - |F_c|)^2/\Sigma w|F_o|^2]^{\frac{1}{2}}$, $w = 1/\sigma^2|F_o|$.

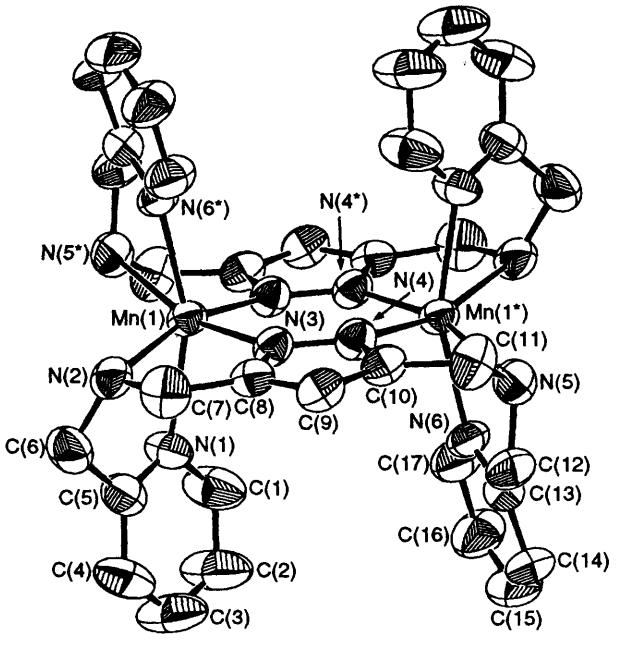

Fig. 2 An ORTEP view of the cationic part of $[Mn_2L^3{}_2][BPh_4]_2 \cdot 2C_6H_5Me$

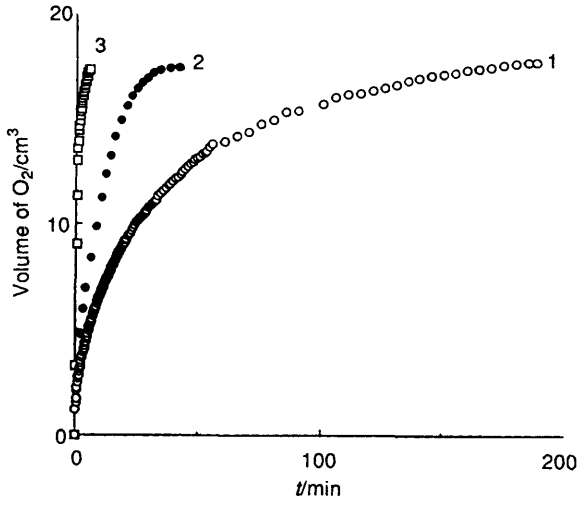

Fig. 3 Time courses of dioxygen evolution on disproportionation of H_2O_2 by complexes **1–3**. Conditions: complex, 5×10^{-6} mol in dmf (2 cm^3); H_2O_2, 1.45×10^{-3} mol (9.9%, 0.5 cm^3); 0 °C

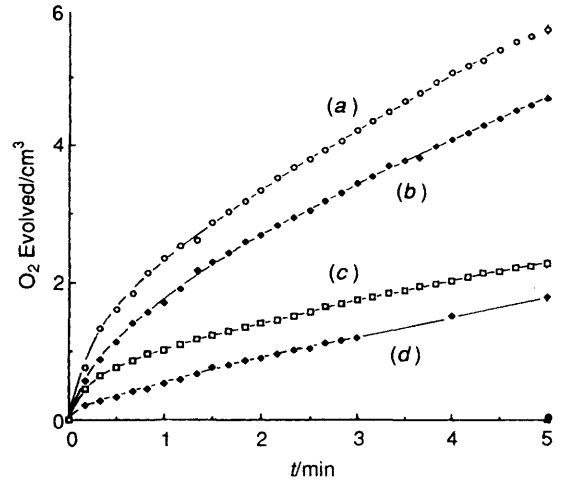

Fig. 4 Dioxygen evolution profiles for the disproportionation of H_2O_2 by complex **1** at different concentrations: H_2O_2, 1.45×10^{-3} mol; complex, (*a*) 2.02×10^{-3}, (*b*) 1.62×10^{-3}, (*c*) 8.18×10^{-4}, (*d*) 4.08×10^{-4} mol dm^{-3}

Table 2 Atomic coordinates of non-hydrogen atoms

Atom	*x*	*y*	*z*	Atom	*x*	*y*	*z*
Mn(1)	0.086 52(6)	0.138 98(6)	0.161 48(8)	C(22)	0.450 4(5)	0.357 6(5)	0.815 7(6)
N(1)	0.216 1(3)	0.106 8(4)	0.227 0(5)	C(23)	0.391 7(4)	0.409 6(4)	0.813 0(5)
N(2)	0.249 6(3)	0.275 3(3)	0.157 8(5)	C(24)	0.283 2(4)	0.541 7(4)	0.834 2(5)
N(3)	0.101 2(3)	0.094 3(3)	−0.038 4(4)	C(25)	0.248 0(5)	0.532 5(5)	0.947 0(6)
N(4)	0.038 8(3)	0.006 2(3)	−0.145 3(4)	C(26)	0.274 5(6)	0.614 8(6)	1.063 8(6)
N(5)	−0.019 7(4)	−0.171 5(4)	−0.357 7(4)	C(27)	0.340 3(6)	0.712 3(6)	1.075 1(7)
N(6)	−0.006 9(3)	−0.231 6(3)	−0.140 5(4)	C(28)	0.377 7(6)	0.726 0(5)	0.969 7(8)
C(1)	0.198 3(5)	0.015 6(5)	0.221 8(8)	C(29)	0.349 4(5)	0.641 7(5)	0.850 5(6)
C(2)	0.275 8(6)	−0.012 3(6)	0.234 6(9)	C(30)	0.270 0(4)	0.473 5(4)	0.570 2(5)
C(3)	0.374 2(6)	0.055 5(6)	0.247 9(9)	C(31)	0.372 9(4)	0.519 3(4)	0.554 3(6)
C(4)	0.398 2(5)	0.152 1(6)	0.252 5(7)	C(32)	0.400 3(5)	0.550 5(4)	0.451 4(6)
C(5)	0.315 8(5)	0.176 3(5)	0.240 4(6)	C(33)	0.324 4(5)	0.534 5(5)	0.353 5(6)
C(6)	0.334 6(4)	0.282 4(5)	0.249 6(6)	C(34)	0.220 9(5)	0.487 1(5)	0.360 8(6)
C(7)	0.262 4(5)	0.256 3(5)	0.019 1(6)	C(35)	0.195 0(4)	0.457 5(4)	0.467 5(6)
C(8)	0.180 9(4)	0.153 6(4)	−0.078 5(6)	C(36)	0.121 3(4)	0.367 5(4)	0.683 0(5)
C(9)	0.171 0(4)	0.105 4(4)	−0.212 5(6)	C(37)	0.080 4(5)	0.274 0(4)	0.697 4(5)
C(10)	0.080 9(4)	0.014 0(4)	−0.249 7(5)	C(38)	−0.024 4(6)	0.218 6(5)	0.695 9(6)
C(11)	0.024 6(5)	−0.075 0(5)	−0.379 6(6)	C(39)	−0.093 7(5)	0.255 3(6)	0.682 1(7)
C(12)	0.063 4(5)	−0.199 3(5)	−0.327 4(6)	C(40)	−0.057 7(5)	0.347 9(6)	0.670 3(6)
C(13)	0.047 3(4)	−0.252 0(4)	−0.230 6(6)	C(41)	0.047 0(5)	0.402 7(4)	0.669 7(6)
C(14)	0.092 1(5)	−0.316 8(5)	−0.229 3(7)	C(42)	0.646 4(8)	0.011(1)	0.129(1)
C(15)	0.084 1(6)	−0.353 7(6)	−0.129 2(8)	C(43)	0.645 2(7)	0.062(1)	0.253(2)
C(16)	0.030 3(6)	−0.332 4(5)	−0.039 0(7)	C(44)	0.659 3(6)	0.157 8(8)	0.292(1)
C(17)	−0.014 4(5)	−0.270 7(5)	−0.048 0(6)	C(45)	0.654 2(9)	0.201(1)	0.419(2)
C(18)	0.314 2(4)	0.379 4(4)	0.706 5(5)	C(46)	0.632(2)	0.154(2)	0.506(2)
C(19)	0.297 9(4)	0.292 5(4)	0.599 2(5)	C(47)	0.622(2)	0.048(3)	0.436(3)
C(20)	0.355 1(5)	0.239 7(4)	0.600 6(6)	C(48)	0.627(1)	0.009(1)	0.330(3)
C(21)	0.432 1(5)	0.273 0(5)	0.708 6(6)	B(1)	0.246 4(5)	0.440 3(5)	0.697 1(6)

Table 3 Selected bond distances (Å) and angles (°)

Mn(1)···Mn(1*)	4.181(2)	Mn(1)–N(1)	2.247(4)
Mn(1)–N(2)	2.406(4)	Mn(1)–N(3)	2.157(4)
Mn(1)–N(4*)	2.133(4)	Mn(1)–N(5*)	2.426(4)
Mn(1)–N(6*)	2.269(4)		
N(1)–Mn(1)–N(2)	75.6(2)	N(1)–Mn(1)–N(3)	105.0(2)
N(1)–Mn(1)–N(4*)	94.6(2)	N(1)–Mn(1)–N(5*)	88.4(2)
N(1)–Mn(1)–N(6*)	158.2(2)	N(2)–Mn(1)–N(3)	73.2(2)
N(2)–Mn(1)–N(4*)	164.0(2)	N(2)–Mn(1)–N(5*)	117.4(2)
N(2)–Mn(1)–N(6*)	101.4(2)	N(3)–Mn(1)–N(4*)	97.7(1)
N(3)–Mn(1)–N(5*)	165.1(1)	N(3)–Mn(1)–N(6*)	94.5(2)
N(4*)–Mn(1)–N(5*)	74.2(2)	N(4*)–Mn(1)–N(6*)	92.4(2)
N(5*)–Mn(1)–N(6*)	73.7(2)		

* Symmetry operation $-x, -y, -z$.

ca. 720 cm^{-1}, is imposed (see Fig. 7, insert). Such an absorption is characteristic of Mn^{IV}=O and the fine structure can be attributed to the ν(Mn=O) vibration coupled to a charge-transfer band from O^{2-} to Mn^{IV}.[31–33] Together with our previous studies,[31–34] this species can be described as $\{Mn^{IV}(=O)\}_2$ which may be involved in the catalysis through the cycle $\{Mn^{III}(OH)\}_2$ to $\{Mn^{IV}(=O)\}_2$ (see Scheme 1).

It should be noted that the characteristic ligand-to-metal charge transfer (l.m.c.t.) band observed in the catalysis by complex **2** is weakened at 0 °C with concomitant fading of the purple colour. This may be explained as follows.[33] If the cycle between the $\{Mn^{III}(OH)\}_2$ and $\{Mn^{IV}(=O)\}_2$ species in the disproportionation of H_2O_2 is rapid, neither of the two species can be detected by any spectroscopy because of their short lifetime. In the presence of **2** the interconversion is slowed at −50 °C allowing detection of the $\{Mn^{IV}=O\}_2$ intermediate by visible spectroscopy. At higher temperatures (0 °C) the interconversion becomes so rapid it is difficult to observe the characteristic l.m.c.t. band. In the presence of **1**, on the other hand, the $\{Mn^{IV}=O\}_2$ intermediate cannot be detected by visible spectroscopy at −50 °C. This is probably due to a short lifetime or low concentration of the $\{Mn^{IV}=O\}_2$ species. This instability (short lifetime), relative to that of **2**, is supported by the high

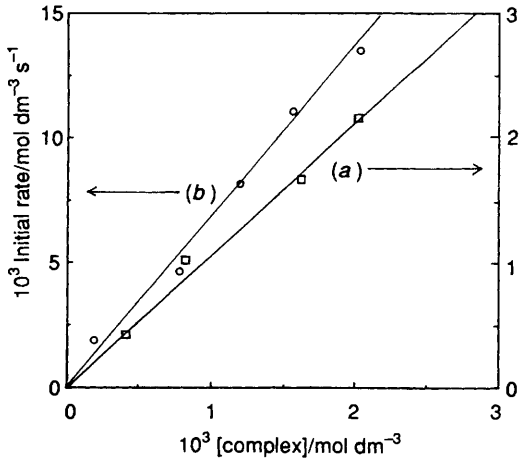

Fig. 5 Correlations between the initial dioxygen evolution rate and the complex concentration in disproportionation of H_2O_2 by **1** (*a*) and **3** (*b*). Conditions for the catalysis by **1**: H_2O_2, 1.45 × 10^{-3} mol; complex, 2.02 × 10^{-3}, 1.62 × 10^{-3}, 8.18 × 10^{-4} and 4.08 × 10^{-4} mol dm^{-3}. Conditions for the catalysis by **3**: H_2O_2, 1.45 × 10^{-3} mol; complex concentration at 2.02 × 10^{-3}, 1.54 × 10^{-3}, 1.18 × 10^{-3}, 8.73 × 10^{-4} and 1.89 × 10^{-4} mol dm^{-3}

oxidation potential of **1** (+1.06 V) compared with that of **2** (+0.84 V). This may also relate to the low catalytic activity of **1** relative to that of **2** as discussed above (see Fig. 2). No ESR signal was observed in the disproportionation of H_2O_2 by **1** or **2**.

The time course of dioxygen evolution in the disproportionation of H_2O_2 by complex **3** is also dependent upon both the complex concentration and that of H_2O_2. In this case the initial rate of evolution is first order in complex concentration [Fig. 4, (*b*)] but second order in $[H_2O_2]$ (Fig. 8); $v = k[\text{complex}][H_2O_2]^2$, k = 29 dm^6 mol^{-2} s^{-1}. The brown reaction mixture showed no distinct visible band at −50 °C, but the

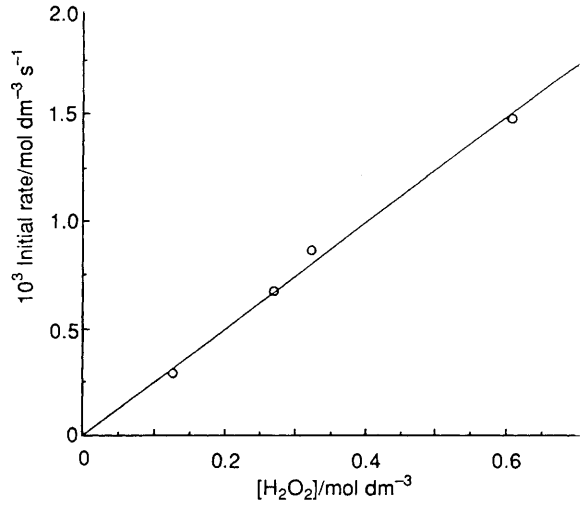

Fig. 6 Correlation between the initial dioxygen evolution rate and the concentration of H_2O_2 in the disproportionation of H_2O_2 by complex **1**: complex, 5×10^{-6} mol; H_2O_2, 6.08×10^{-1}, 3.24×10^{-1}, 2.68×10^{-1}, and 1.25×10^{-1} mol dm^{-3}

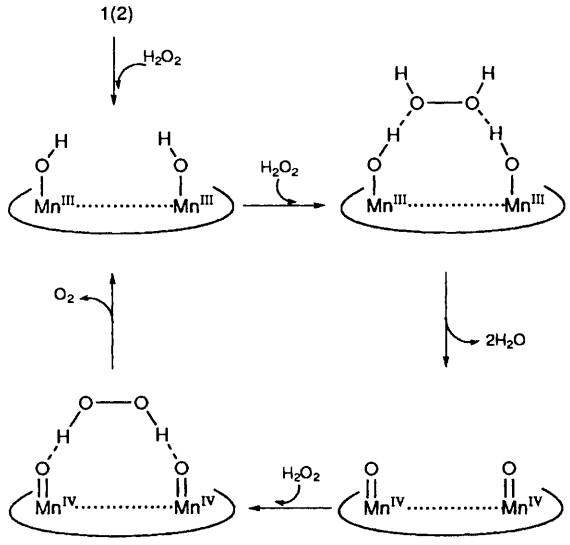

Scheme 1 Probable mechanism for disproportionation of H_2O_2 by complexes **1** and **2**

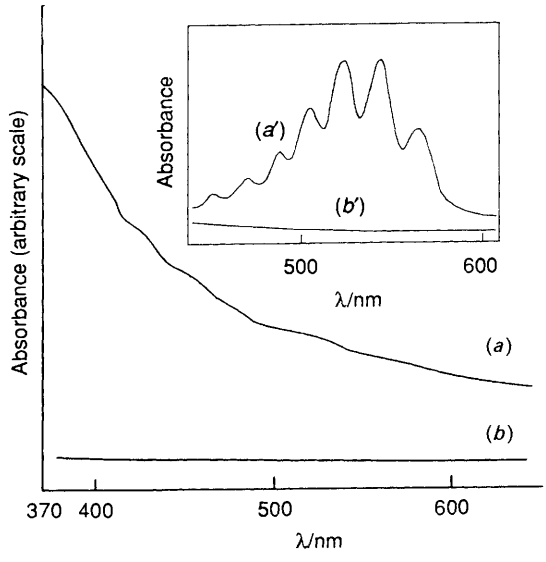

Fig. 7 Visible spectra of complex **1** measured at −50 °C in the presence (*a*) and absence (*b*) of H_2O_2. The insert shows the corresponding spectra for **2**

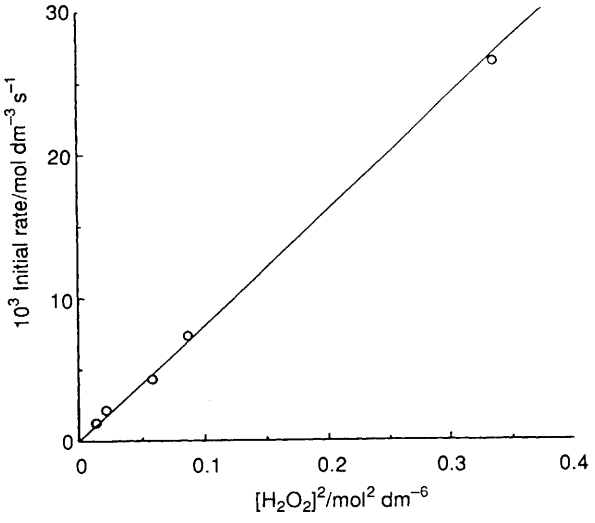

Fig. 8 Correlation between the initial dioxygen evolution rate and $[H_2O_2]^2$ in disproportionation of H_2O_2 by complex **3**: complex, 5×10^{-6} mol; H_2O_2, 5.80×10^{-1}, 2.95×10^{-1}, 2.41×10^{-1}, 1.45×10^{-1} and 1.18×10^{-1} mol dm^{-3}

visible region of the spectrum clearly showed an increase in intensity. No ESR signal was observed.

Despite the lack of visible and ESR spectroscopic evidence for the active intermediate involved in the disproportionation of H_2O_2 by complex **3**, the kinetic study suggests the involvement of a 1:2 adduct between **3** and H_2O_2. In this context the apical pyridyl donors of **3** must be replaced with two H_2O_2 molecules. In the disproportionation of H_2O_2 by dinuclear copper(II) complexes, Nishida and co-workers [35,36] have proposed the formation of a 1:2 Cu_2:H_2O_2 adduct with two bridging H_2O_2 molecules above and below the Cu_2 core. They propose a two-electron transfer from one H_2O_2 to another through the Cu_2 core without any change in oxidation state of the latter. In the disproportionation of H_2O_2 by **3** a higher oxidation state of Mn is involved judged from the colouration of the reaction mixture. However, the detailed mechanism of the catalase-like function of **3** remains to be elucidated in terms of stereochemical and electronic modulations of the dinuclear Mn_2 core.

Acknowledgements

This work was supported by a Grant-in-Aid (No. 07454178) from The Ministry of Education, Science and Culture, Japan. Thanks are also due to Mr M. Ohba for the help with magnetic measurements.

References

1 D. E. Fenton and H. Ōkawa, *Perspectives on Bioinorganic Chemistry*, ed. R. Hay, J. Dilworth and K. Nolan, London, 1993, vol. 2, p. 82.
2 W. P. J. Gaykema, A. Volbeda and W. G. J. Hol, *J. Mol. Biol.*, 1985, **187**, 255; A. Volbeda and W. G. J. Hol, *J. Mol. Biol.*, 1989, **209**, 249.
3 V. V. Baynin, A. A. Vagin, V. R. Melik-Adamyan, A. I. Grebenko, S. V. Khangulov, A. N. Popov, M. E. Andrianova and B. K. Vainshtein, *Dokl. Akad. Nauk SSSR*, 1986, **288**, 877.
4 S. Trofimenko, *Chem. Rev.*, 1972, **72**, 497; M. Inoue and M. Kubo, *Coord. Chem. Rev.*, 1976, **21**, 1.
5 P. W. Ball and A. B. Blake, *J. Chem. Soc. A*, 1969, 1415.
6 M. G. B. Drew, P. C. Yates, F. S. Esho, J. T.-Grimshaw, A. Lavery, K. P. McKillop, S. M. Nelson and J. Nelson, *J. Chem. Soc., Dalton Trans.*, 1988, 2995.

7 J. Casabo, J. Pons, K. S Siddiqi, F. Texidor, E. Molins and C. Miravitlles, *J. Chem. Soc., Dalton Trans.*, 1989, 1401.
8 D. Ajo, A. Bencini and F. Mani, *Inorg. Chem.*, 1988, **27**, 2437.
9 P. M. Slangen, P. J. van Koningsbruggen, K. Goubitz, J. G. Haasnoot and J. Reedijk, *Inorg. Chem.*, 1994, **33**, 1121; W. M. E. K. Oudenniel, R. A. G. de Graaff, J. P. Haasnoot, R. Prins and J. Reedijk, *Inorg. Chem.*, 1989, **28**, 1128; A. Bencini, D. Gatteschi, C. Zanchini, J. G. Haasnoot and J. Reedijk, *J. Am. Chem. Soc.*, 1987, **109**, 2926; R. Prins, R. A. G. de Graaff, J. G. Haasnoot, C. Vader and J. Reedijk, *J. Chem. Soc., Chem. Commun.*, 1986, 1430; A. Bencini, D. Gatteschi, C. Zanchini, J. G. Haasnoot, R. Prins and J. Reedijk, *Inorg. Chem.*, 1985, **24**, 2812.
10 J. E. Andrew and A. B. Blake, *J. Chem. Soc. A*, 1969, 1408; P. W. Ball and A. B. Blake, *J. Chem. Soc., Dalton Trans.*, 1974, 852; L. K. Thompson, T. C. Woon, D. B. Murphy, E. J. Gabe, F. L. Lee and Y. Le Page, *Inorg. Chem.*, 1985, **24**, 4719.
11 P. J. Steel, *Coord. Chem. Rev.*, 1990, **106**, 221.
12 T. Otieno, S. J. Retting, R. C. Thompson and J. Trotter, *Inorg. Chem.*, 1995, **34**, 1718.
13 L. K. Thompson, F. W. Hartstock, P. Robichaud and A. W. Hanson, *Can. J. Chem.*, 1984, **62**, 2755.
14 T. Kamiusuki, H. Ōkawa, E. Kitaura, M. Koikawa, N. Matsumoto and S. Kida, *J. Chem. Soc., Dalton Trans.*, 1989, 2077.
15 T. Kamiusuki, H. Ōkawa, N. Matsumoto and S. Kida, *J. Chem. Soc., Dalton Trans.*, 1990, 195.
16 T. Kamiusuki, H. Ōkawa, E. Kitaura, K. Inoue and S. Kida, *Inorg. Chim. Acta*, 1991, **179**, 139.
17 T. Kamiusuki, H. Ōkawa, K. Inoue, N. Matsumoto, M. Kodera and S. Kida, *J. Coord. Chem.*, 1991, **23**, 201.
18 K. Shindo, Y. Mori, K. Motoda, H. Sakiyama, N. Matsumoto and H. Ōkawa, *Inorg. Chem.*, 1992, **31**, 4987.
19 N. F. Curtis, *J. Chem. Soc.*, 1961, 3147.
20 E. A. Boudreaux and L. N. Mulay, *Theory and Application of Molecular Paramagnetism*, Wiley, New York, 1976, p. 491.
21 D. T. Cromer and J. T. Waber, *International Tables for X-Ray Crystallography*, Kynoch Press, Birmingham, 1974, vol. 4.
22 J. A. Ibers and W. C. Hamilton, *Acta Crystallogr.*, 1964, **17**, 781.
23 D. C. Creagh and W. J. McAuley, *International Tables for X-Ray Crystallography*, ed. A. J. C. Wilson, Kluwer, Boston, 1992, pp. 219–222.
24 D. C. Creagh and H. H. Hubbell, *International Tables for X-Ray Crystallography*, ed. A. J. C. Wilson, Kluwer, Boston, 1992, pp. 200–206.
25 TEXSAN, Structure Analysis Package, Molecular Structure Corporation, Houston, TX, 1985.
26 G. B. Deacon and R. J. Phillips, *Coord. Chem. Rev.*, 1980, **33**, 227.
27 W. J. Geary, *Coord. Chem. Rev.*, 1971, **7**, 81.
28 C. K. Johnson, ORTEP, ORNL 3794, Oak Ridge National Laboratory, Oak Ridge, TN, 1965.
29 K. Yano and I. Fridovich, *J. Biol. Chem.*, 1983, **258**, 6015.
30 G. S. Allgood and J. J. Perry, *J. Bacteriol.*, 1986, **168**, 563.
31 H. Sakiyama, H. Ōkawa and R. Isobe, *J. Chem. Soc., Chem. Commun.*, 1993, 882.
32 C. Higuchi, H. Sakiyama, H. Ōkawa, R. Isobe and D. E. Fenton, *J. Chem. Soc., Dalton Trans.*, 1994, 1097.
33 H. Wada, K. Motoda, M. Ohba, H. Sakiyama, N. Matsumoto and H. Ōkawa, *Bull. Chem. Soc. Jpn.*, 1995, **68**, 1105.
34 H. Sakiyama, H. Ōkawa and M. Suzuki, *J. Chem. Soc., Dalton Trans.*, 1993, 3823.
35 N. Oishi, M. Takeuchi, Y. Nishida and S. Kida, *Bull. Chem. Soc. Jpn.*, 1982, **55**, 3747.
36 N. Oishi, M. Takeuchi, Y. Nishida and S. Kida, *Polyhedron*, 1984, **3**, 157.

Received 11*th May* 1995; *Paper* 5/03003J